Journal of The Electrochemical Society, **156** (8) A688-A693 (2009)
0013-4651/2009/156(8)/A688/6/$25.00 © The Electrochemical Society

Thermoelectrochemically Activated MoO_2 Powder Electrode for Lithium Secondary Batteries

Jun H. Ku, Yoon S. Jung,[a] Kyu T. Lee,[b] Chang H. Kim, and Seung M. Oh[*,z]

Department of Chemical and Biological Engineering and Research Center for Energy Conversion and Storage, Seoul National University, Seoul 151-744, South Korea

The high temperature lithiation behavior of the MoO_2 electrode is examined, which is lithiated by one-electron reduction (by addition reaction) at room temperature. At elevated temperatures, this electrode is lithiated with four-electron reduction by addition and continued conversion reaction. As a result of four-electron reduction, the initial crystalline MoO_2 phase is decomposed into a nanosized mixture of metallic Mo and Li_2O, which is in turn converted to nanosized MoO_2 upon forthcoming delithiation. An interesting feature here is that as-generated nanosized MoO_2 is now fully lithiated up to four-electron reduction even at room temperature. This phenomenon is named "thermoelectrochemical activation" because the extension from one- to four-electron reduction is achieved by a simple charge–discharge cycling made at elevated temperatures. The thermoelectrochemically activated MoO_2 electrode delivers a reversible specific capacity that is close to the theoretical four-electron capacity (838 mAh g^{-1}) with an excellent cycle performance at room temperature.
 [DOI: 10.1149/1.3141670]

Manuscript submitted February 24, 2009; revised manuscript received April 27, 2009. Published June 4, 2009.

Since the commercialization of lithium-ion batteries (LIBs) by SONY Corporation in the early 1990s, LIBs have been used as the major power source for portable electronic devices.[1,2] The recent issues of oil price and global warming drive a continuous development of cleaner and more fuel-efficient hybrid electric vehicles (HEVs), in which LIBs with their superior performance to nickel–metal hydride cells are now being considered as the future power source. The existing LIB technologies, however, still have serious cost and performance limitations with respect to energy density, safety, and cycle life, which hinders the widespread use of sophisticated electronic devices and HEVs.

To increase the energy density of LIBs, many electrode materials containing redox centers that accept more than one electron over a small voltage window have been highly sought. In this sense, a series of transition-metal oxides (M_xO_y with M = Fe, Co, Ni, Cu, etc.) seems to be one of the candidate materials because the transition-metal components in these oxides are converted to their elemental state by more than one-electron reduction.[3] As a result of this reduction reaction, nanosized metal particles that are dispersed in the Li_2O matrix are formed (this is called conversion reaction) but restored to the original oxides by delithiation.[3-6] The number of electrons involved in this charge–discharge process is determined by the oxidation state of metallic components; for instance, four electrons for MoO_2. This conversion reaction is contrasted by the addition-type lithiation, in which the number of electrons involved in the redox reactions is commonly limited to less than 1 because Li inserts into the vacant sites of metal oxide frameworks without M–O bond cleavage.[7-16]

When considered as the negative electrode for LIBs, the lithiation of metal oxides should take place at >0.0 V (vs Li/Li^+) to prevent Li plating. Within this voltage window, the room-temperature lithiation behavior of metal oxides, which has been reported, can be classified into four groups: The first group does not show any lithiation activity; NbO and TiO.[11] The extent of lithiation for the second group is limited to the addition-type reaction; TiO_2,[7,14] V_2O_5,[10,13] and MoO_2.[8,9,12,13,16] The third group is lithiated by the addition-type reaction in advance, which is followed by the conversion reaction; RuO_2.[17] The final group is lithiated by the conversion reaction without the addition-type intermediate step; CoO, NiO, and Cu_2O.[3,18] The controlling factors for the room-temperature lithiation behavior must be, among others, the lattice structure of metal oxides, thermodynamic and kinetic parameters, and charge–discharge rates. That is, the lattice structure of oxides should provide vacant sites for Li for the addition-type lithiation. In a thermodynamic point of view, the equilibrium potential for lithiation should be at least >0.0 V. Even if this thermodynamic condition is met, the lithiation should not be hindered by any kinetic reasons. Otherwise, lithiation sometimes takes place below 0.0 V under transient charge–discharge cycling conditions, in particular, under a high rate cycling condition.

According to the literature, the lithiation of the MoO_2 electrode is limited to the addition reaction with one-electron reduction at room temperature.[8,9,12,13,16] That is, the conversion reaction does not take place in a normal cycling condition. Given that the conversion reaction is thermodynamically feasible at room temperature,[11] the absence of this reaction must be attributed to a slower kinetics. Intuitively, one way to increase the conversion reaction rate is to raise the working temperature. An enlargement of surface and defect sites must be another measure to facilitate the conversion reaction because this reaction proceeds through heterogeneous charge-transfer reaction and solid-state Li^+- or O^{2-}-ion diffusion.[5,11,19] With these two premises in mind, we examined the conversion reaction activity of the MoO_2 electrode at elevated temperatures. We also examined whether or not the conversion reaction is facilitated by ballmilling of the initial MoO_2 powder, with which an increase in the surface area and defect sites can be assumed.

Experimental

For the X-ray diffraction (XRD) and Raman and X-ray photoelectron spectroscopy (XPS) studies, a MoO_2-embedded Ag foil electrode was prepared by pressing (170 MPa) the MoO_2 powder (Aldrich) that was spread on a piece of Ag foil (1.0 cm^2 and ca. 0.25 mm thick).[20] With this configuration, any spectroscopic interferences that came from carbon additive and polymer binder was avoided. For the galvanostatic discharge/charge cycling, a composite electrode was prepared by spreading the slurry of the MoO_2 powder, Super-P (as a carbon additive for conductivity enhancement), and polyvinylidene fluoride (as a binder) (70:20:10 in weight ratio) on a piece of Cu foil, which was followed by drying in vacuum at 120°C for 12 h. The electrode plate was then pressed to enhance the interparticle contact and to ensure better adhesion to the current collector.

XRD patterns were obtained using a D8-Bruker diffractometer equipped with Cu Kα radiation (1.54056 Å). For the sample preparation, the cells were disassembled and electrodes were rinsed with dimethyl carbonate (DMC) and dried in an argon-filled dry box. All the XRD patterns were recorded at 3 kV and 20 mA using a continuous scanning mode with 1.0° min^{-1}. XPS measurements were

* Electrochemical Society Active Member.
[a] Present address: Department of Mechanical Engineering, University of Texas at Austin, Austin, TX 78712, USA.
[b] Present address: Department of Chemistry, University of Waterloo, Ontario N2L3G1, Canada.
[z] E-mail: seungoh@snu.ac.kr

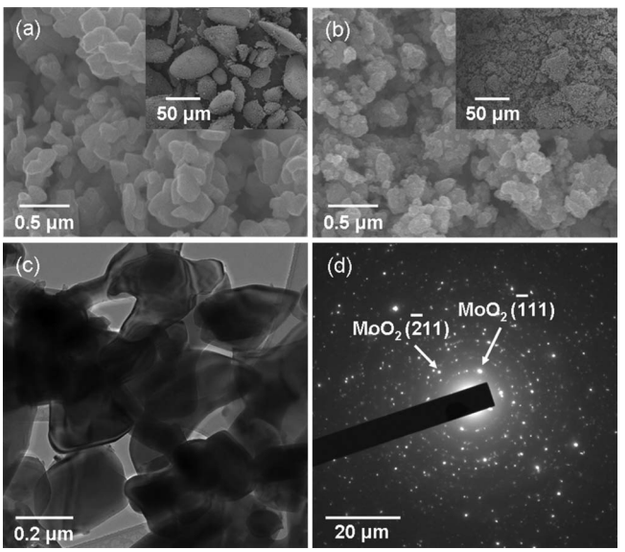

Figure 1. The FE-SEM images of the (a) raw MoO_2 and (b) ballmilled MoO_2. The HR-TEM image of the (c) raw MoO_2 and (d) SAED pattern.

made in an ultrahigh vacuum multipurpose surface analysis system (Sigma Probe, Thermo, U.K.) using an Al Kα (1486.6 eV) anode operating at constant power (15 kV and 10 mA). During the data acquisition, the constant energy mode was employed at a pass energy of 30 eV and a step of 0.1 eV. Depth analysis was made by etching the samples with argon-ion beam (accelerating voltage of 3 kV and ion-beam current of 1 μA). For the postmortem high resolution transmission electron microscope (HR-TEM) analysis, the cells were disassembled and the powders in electrodes were dispersed in DMC by sonication in an argon-filled dry box before loading on the transmission electron microscopy (TEM) grid. All the procedures were carried out under inert atmosphere and the samples were transferred using a hermitically sealed bottle. TEM images and selected area electron diffraction (SAED) patterns were obtained using JEOL JEM-2100F and 2010 at 200 kV of acceleration voltage. The Raman study was made with a LabRam HR (Jobin-Yvon Co., France) spectrometer with a 514.5 nm Ar^+ laser. Signals were collected by using a multichannel charge-coupled device detector cooled to 140 K. The Brunauer, Emmett, and Teller (BET) surface area was measured from the N_2 adsorption isotherms that were obtained with a gas adsorption analyzer (Micromeritics, ASAP 2010). The particle morphology was examined using a field-emission scanning electron microscope (FE-SEM) (JEOL JSM-6700F).

The galvanostatic discharge/charge cycling was made in a temperature-controlled oven using a two-electrode 2032-type coin cell. Li metal foil was used as the counter electrode. To prevent Li plating and lithiation to Ag substrate, the lower cutoff voltage was varied according to the working temperature and the used substrate; 0.1–3.0 V (vs Li/Li^+) (Cu substrate, 120°C), 0.16–3.0 V (vs Li/Li^+) (Ag substrate, 120°C), and 0.05–3.0 V (vs Li/Li^+) (Cu substrate, 55°C), respectively. Different electrolytes were used according to the working temperatures: 1.0 M $LiPF_6$ dissolved in a mixture of ethylene carbonate (EC) and DMC (1:2 in volume ratio) at ≤75°C and 1.0 M lithium bis(oxalatoborate) in a mixture of EC and diethyl carbonate (1:1 in volume ratio) at ≥85°C. As the separator, a porous polypropylene (PP) film was used at ≤75°C but a glass fiber sheet at ≥85°C because the PP was deformed at ≥85°C. In this paper, lithiation was expressed as discharging, whereas delithiation was expressed as charging.

Results and Discussion

Figure 1 shows the FE-SEM images of the raw and ballmilled MoO_2 powder. The HR-TEM image and SAED pattern that are obtained with the raw MoO_2 are also included. The apparent size of the raw MoO_2 particles is 10–50 μm (inset of Fig. 1a), but each particle comprises the primary particles of 0.2–0.3 μm in size (Fig. 1a). The HR-TEM image ensures that the size of the primary particles in the raw MoO_2 is in the range of 0.2–0.3 μm (Fig. 1c). The raw MoO_2 powder is highly crystalline as seen from the SAED pattern, in which intense lattice fringes can be identified (Fig. 1d). The size reduction by ballmilling is ascertained from the FE-SEM image taken with the ballmilled sample (Fig. 1b), in which the primary particles of 0.1–0.2 μm can be located. From the irregular-shaped particle morphology and roughened surface of the ballmilled powder, an increase in the surface area and defect sites can be assumed.

Figure 2 shows the first galvanostatic discharge (lithiation, downward profiles) and charge (delithiation, upward) voltage profiles of the MoO_2/Li cell and the XRD patterns of MoO_2 electrodes obtained at 25 and 120°C. At 25°C (Fig. 2a), the MoO_2 electrode accepts ca. 1.7 Li/Mo but releases ca. 1.0 Li/Mo. The cyclic voltammograms shown in the inset illustrate that reversible Li^+ uptake/extraction takes place at 1.0–2.0 V, but irreversible ones at two voltage regions (>2.0 and <1.0 V). The irreversible reaction at >2.0 V occurs only in the first cycle (solid line), but that appeared at <1.0 V is still observed in the second cycle (dotted line). Further study is continuing in this laboratory to identify the nature of these irreversible reactions. The XRD data (Fig. 2c) illustrate the Li^+ uptake/extraction mechanism prevailing at 25°C.[8,9,12,13] The most intense $(\bar{1}11)$ diffraction line of the MoO_2 phase (monoclinic, space group = $P2_1/c$, JCPDS no. 00-032-0671) steadily moves to the smaller angle (scans 1–3) in the earlier stage of lithiation, indicative of a single-phase lithiation. A careful inspection on the diffraction peaks evolved at 24–25° (scans 4–6) reveals that the peak at 24.5° grows at the expense of the peak at 24.8°, indicative of the presence of a two-phase reaction in this voltage region. The delithiation proceeds by the reverse order: Two-phase reaction (scans 6 and 7) and subsequent single-phase reaction (scans 8 and 9).

The fully lithiated MoO_2 phase (scan 6) has been assigned to $Li_{0.98}MoO_2$ (JCPDS no. 01-087-0392) in this work. The other phase having a very close composition ($LiMoO_2$) can be discarded because even the most intense diffraction peak at $2\theta = 17.2°$ for this phase is absent in this work.[12] The formation of $Li_{0.98}MoO_2$ can be confirmed from the data in Fig. 2a. This electrode is lithiated by 1.7 Li/Mo, but the reversible one amounts to ca. 1.0 Li/Mo if the irreversible contribution at <1.0 V (ca. 0.7 Li/Mo) is subtracted. Also the delithiation capacity is very close to 1.0 Li/Mo. In short, the MoO_2 electrode is lithiated by an addition-type reaction with one-electron reduction at 25°C and restores to its initial crystalline MoO_2 phase (scan 9). The maintenance of structural framework and no decomposition into the metallic state reflect that the conversion reaction does not take place at 25°C.

To see if the conversion reaction occurs at elevated temperatures, the working temperature was varied from 25 to 120°C with 10°C intervals. The voltage profiles observed below 75°C were similar to that shown in Fig. 2a, whereas a somewhat different voltage profile was obtained at 85–120°C. The voltage profile obtained at 120°C is represented in Fig. 2b. The most apparent difference to that obtained at 25°C (Fig. 2a) is the additional voltage plateau evolving at 0.23–0.16 V with ca. 2.8 Li uptake (between scans 3 and 4). As a result of this extra lithiation, total lithiation capacity amounts to ca. 5.0 Li/Mo. The nature of lithiation reaction occurring in this plateau region has been identified by an XRD study (Fig. 2d). Before approaching the plateau region (scans 1–3), the MoO_2 phase experiences a single-phase reduction (scans 1 and 2) and then a two-phase reduction (scans 2 and 3) to be $Li_{0.98}MoO_2$ (scan 3), which is the same structural change observed at 25°C (Fig. 2c). Further lithiation at the plateau region gives rise to a featureless XRD pattern (scan 4), indicating that the lithiated products are amorphous or extremely small in size. As will be seen in the later section, the lithiated product is nanosized metallic Mo that carries an appreciable crystallinity.

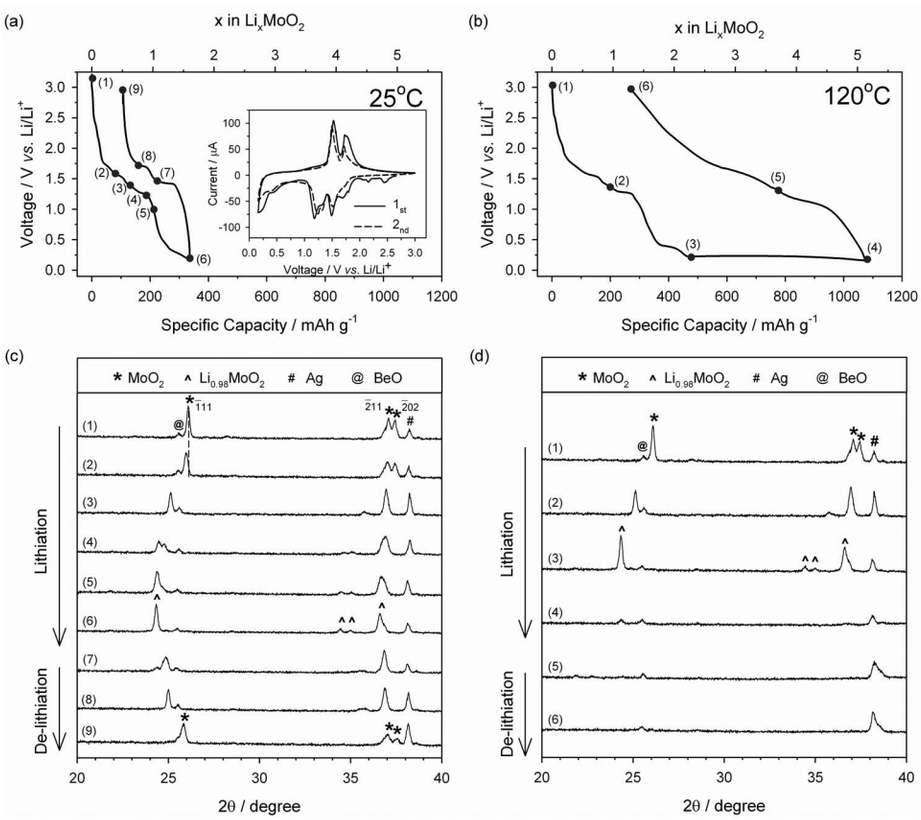

Figure 2. The first galvanostatic discharge/charge voltage profiles of the raw MoO_2/Li cell obtained (a) at 25 and (b) at 120°C. Specific current = 100 mA g^{-1}. The lower cutoff voltage was fixed at 0.16 V because the lithiation to Ag substrate takes place below this voltage. The XRD patterns recorded with the raw MoO_2 electrode at (c) 25 and (d) 120°C. The numbers denote the positions at which the XRD patterns were taken. The diffraction peaks from the Ag substrate and beryllium window in the electrochemical XRD cell also appeared.

Decomposition into nanosized metal particles is a common observation for transition-metal oxides that undergo a conversion-type lithiation reaction.[3-6,21] The evolution of the conversion reaction at the plateau region has been further confirmed by calculating the lithiation/delithiation capacity. In theory, 3.0 Li/Mo is required for the conversion reaction because 1.0 Li/Mo has already been consumed for the addition reaction. The experimentally observed lithiation capacity is 2.8 Li/Mo at the plateau region (0.23–0.16 V in Fig. 2b), which is close to the theoretical value. Another revealing feature in Fig. 2d is that the featureless XRD pattern is maintained upon delithiation (scans 5 and 6), reflecting that the delithiated products and any intermediates are also nanosized in nature.

The four-electron reduction to metallic Mo (one electron by addition and three electron by conversion reaction) and four-electron oxidation back to MoO_2 have been evidenced by XPS study. The MoO_2 electrode that is lithiated down to 0.16 V clearly shows the presence of metallic Mo and the delithiated sample up to 3.0 V the MoO_2 phase (Fig. 3a). The restoration to the MoO_2 phase is further confirmed by Raman study (Fig. 3b). The delithiated electrode gives the same Raman peaks to those of the initial MoO_2 sample,[22] suggesting that the Mo species generated by delithiation is nothing but the MoO_2 phase. One notable feature here is the redshift (5–10 cm^{-1}) for the delithiated MoO_2, which means that the Mo–O bond in the delithiated MoO_2 is weaker than that for the initial one.[17,23] Further discussion will be made later.

The conversion reaction in metal oxides requires a heterogeneous charge transfer at the interfaces, Li^+ and O^{2-} diffusion in solid state, and M–O bond cleavage. Intuitively, these processes play as an activation barrier for the conversion reaction. For the initial MoO_2, the activation barrier is so large that the conversion reaction cannot take place at above 0.16 V (the cutoff limit) under the present cycling condition at room temperature (Fig. 2a) even if the reaction is thermodynamically feasible, but this reaction becomes possible when the working temperature is higher than the onset temperature (ca. 85°C). It is now interesting to see whether or not the same kinetic barrier prevails in the nanosized MoO_2 phase (less than 10 nm as seen later). Figure 4a compares the lithiation voltage profiles obtained in the first and second cycles at 120°C. The first profile corresponds to that for the initial MoO_2, whereas the second one for the nanosized MoO_2. An apparent feature in Fig. 4a is the higher plateau voltage for the conversion reaction (0.47 V) in the second cycle, reflecting that the conversion reaction is more facilitated in the nanosized MoO_2. This favorable feature resulted from both thermodynamic (equilibrium potential for conversion reaction) and kinetic contributions (polarization). The galvanostatic intermittent titration technique (GITT) experiment made at the plateau region (Fig. 4b), however, illustrates that the kinetic contribution is dominant over the thermodynamic ones. That is, the quasi-equilibrium potential for the conversion reaction for the initial MoO_2 (the average value of six open circles) is 0.77 V, which is comparable to that (0.74 V) for the nanosized one. In contrast, there appears an appreciable difference in the overpotential values (difference between the quasi-equilibrium potential and transient value); 0.54 V for the initial MoO_2 and 0.27 V for the nanosized one. Clearly, the facilitated conversion reaction for the latter resulted from an enhanced kinetics. As mentioned above, the heterogeneous charge transfer and solid-state Li^+ or O^{2-} diffusion may be the kinetic barriers that impede the conversion reaction. Along this line, the enhanced kinetics for the nanosized MoO_2 can be ascribed to a transformation from the submicron-sized (0.2–0.3 μm for the raw MoO_2) to the nanosized particles.[3-5,17] The downsizing of particles and increase in defect sites in the latter seem to be favorable for the heterogeneous charge transfer and solid-state ion diffusion. Another kinetic barrier for the conversion reaction must be the M–O bond cleavage. In this sense, the enhanced conversion activity can also be attributed to a weaker Mo–O bond strength for the nanosized MoO_2, which has been evidenced by the redshift in the Raman spectra (Fig. 3b).

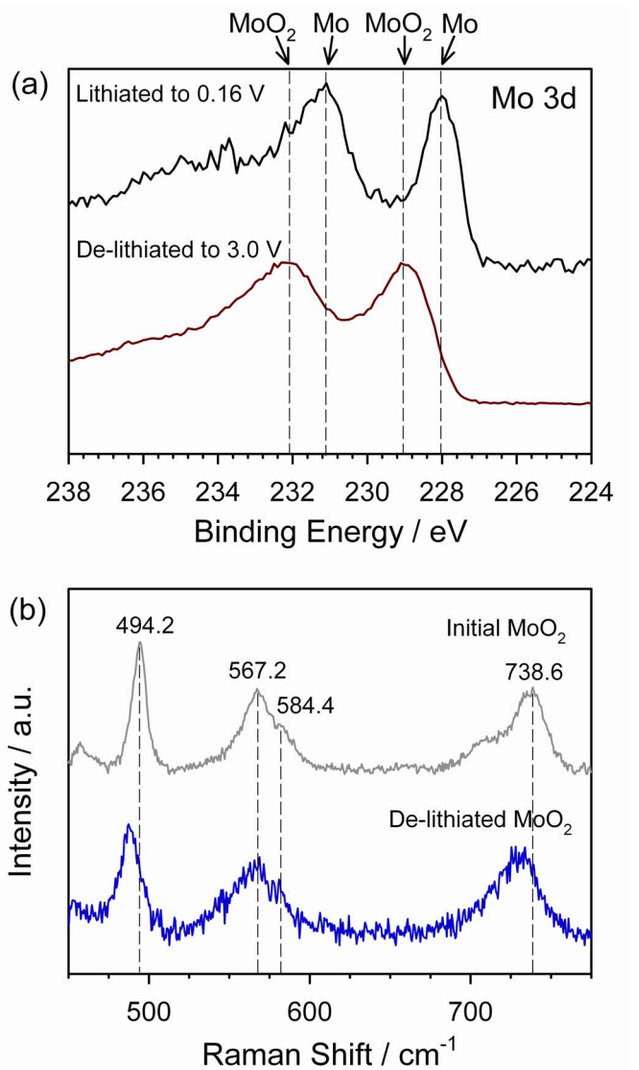

Figure 3. (Color online) (a) The Mo 3d XPS spectra obtained with the MoO_2 electrode cycled at 120°C. The binding energy of photoelectrons; Mo $3d_{3/2}$ = 228 eV and Mo $3d_{5/2}$ = 231.2 eV for Mo metal and Mo $3d_{3/2}$ = 229 eV and Mo $3d_{5/2}$ = 232.2 eV for MoO_2. The samples were etched by argon-ion sputtering to remove the surface film. (b) The Raman spectra recorded with the raw MoO_2 and nanosized MoO_2 electrodes that were cycled at 120°C.

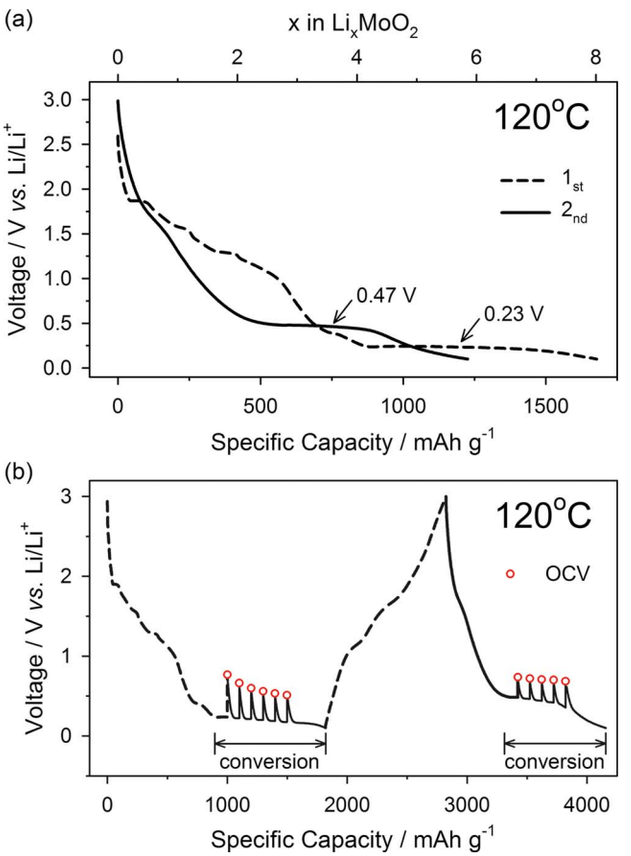

Figure 4. (Color online) (a) The first and second galvanostatic discharge voltage profiles obtained with the MoO_2/Li cell at 120°C. The voltage where the conversion reaction occurs is indicated. (b) The first and second transient voltage profiles overlapped with the GITT data. The open-circuit voltages (open circles) were obtained by resting the cells for 24 h in each transient period.

The finding that the nanosized MoO_2 electrode exhibits an enhanced conversion activity led us to examine its lithiation activity at room temperature. To this end, a nanosized MoO_2 phase was generated by cycling at 120°C (dotted line in Fig. 5a), and then cycling at 25°C (solid line). Surprisingly, the extent of lithiation that was limited to the addition-type reaction at room temperature (Fig. 2a) is now extended to the conversion reaction. That is, the nanosized MoO_2 electrode is lithiated by an addition reaction at 2.0–1.0 V, which is followed by a conversion reaction at the 0.28 V plateau region (solid line in Fig. 5a). The lithiation and delithiation capacities amount to 912 and 842 mAh g^{-1}, respectively, which is close to the theoretical four-electron redox capacity (838 mAh g^{-1}). The observed capacity is slightly larger than the theoretical value due to the contribution from carbon additive (Super P). In short, the submicron-sized MoO_2 powder that reacts by one-electron reduction at room temperature now reacts with four after being converted to the nanosized one by a cycling at 120°C. This phenomenon is named thermoelectrochemical activation because the electrode is activated from one- to four-electron reduction by a charge–discharge cycling made at elevated temperatures. Figure 5b shows the voltage profile that was obtained by another activation process, in which thermoelectrochemical activation was performed only by a lithiation at 120°C (dotted line). The forthcoming voltage profile obtained at 25°C (solid line) looks similar to that shown in Fig. 5a. This explains that the essential step for activation is the conversion process (↓) made at elevated temperatures, during which the initial bulkier MoO_2 particles are decomposed into the nanosized mixture of Mo and Li_2O. That is, once the nanosized Mo/Li_2O mixture is generated, the transformation to nanosized MoO_2 is ensured regardless of the delithiation temperature. Figure 5c presents the cycle performance of initial MoO_2 and two electrochemically activated ones (TEA1 and TEA2). The initial MoO_2 electrode delivers one-electron redox capacity with significant capacity decay. In contrast, two electrochemically activated ones show an excellent cycle performance with four-electron redox capacity.

As mentioned above, the onset temperature for the conversion reaction is near 85°C under the present cycling condition for the raw MoO_2 powder electrode. Upon considering that surface area and defect sites are important variables to affect the kinetics of conversion reaction, it is readily expected that the onset temperature can be lowered by ballmilling the raw MoO_2 powder. As shown in Fig. 1b, the initial MoO_2 particles (0.2–0.3 μm in size) are mechanically crushed to be irregular-shaped ones with a decrease in size (0.1–0.2 μm). The separate BET measurement illustrates a slight

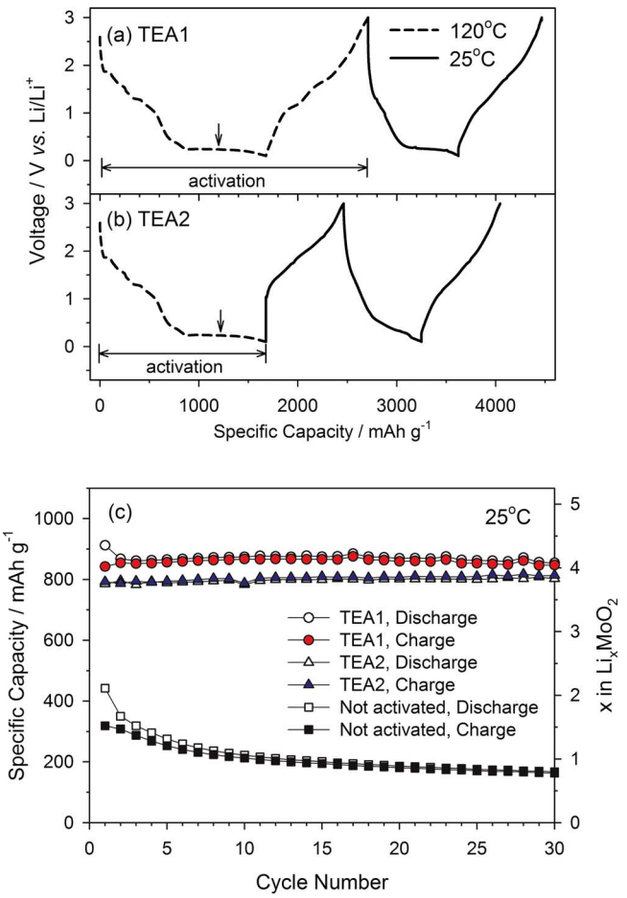

Figure 5. (Color online) The galvanostatic discharge/charge voltage profiles obtained with the MoO_2/Li cells at 25°C (solid line). A composite electrode comprising MoO_2 powder, carbon additive, and polymer binder was used. Two different cycling modes were applied for thermoelectrochemical activation (dotted line); (a) discharge/charge at 120°C and (b) discharge only at 120°C. (c) Cycle performance obtained with the activated and nonactivated MoO_2/Li cells at 25°C. Specific current = 100 mA g^{-1}.

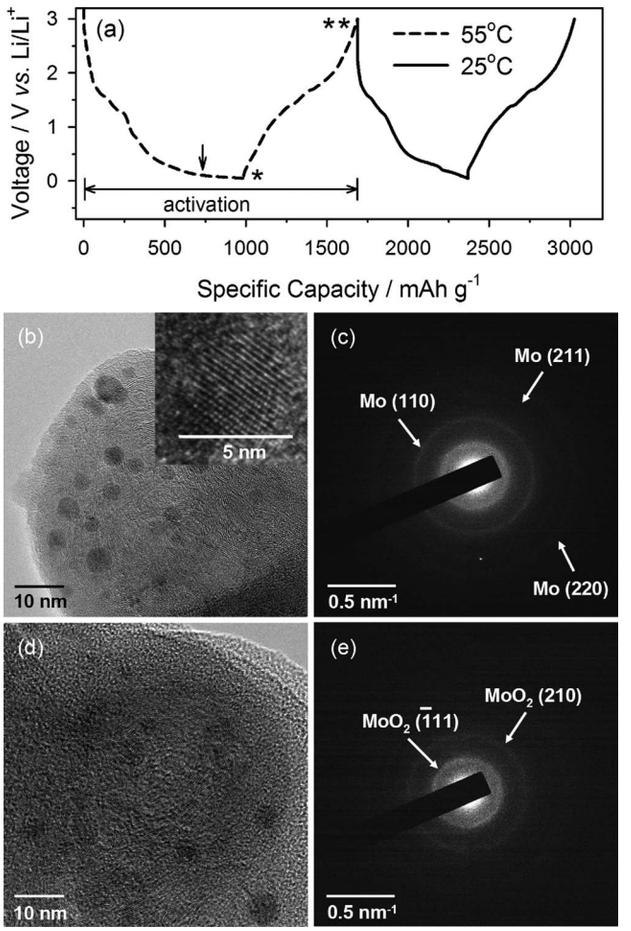

Figure 6. (a) The galvanostatic discharge/charge voltage profiles obtained with the ballmilled MoO_2/Li cell at 55°C (dotted line) and 25°C (solid line). Specific current = 100 mA g^{-1}. The voltage profiles obtained at ≤45°C were largely the same as that shown in Fig. 2a, indicating that the onset temperature for thermoelectrochemical activation is near 55°C for the ballmilled MoO_2. The HR-TEM images and SAED patterns obtained [(b) and (c), respectively] after a full lithiation and [(d) and (e), respectively] after a full delithiation.

increase in the surface area (from 4.4 to 8.7 m^2 g^{-1}) by ballmilling. Figure 6a displays the voltage profiles taken before and after the thermoelectrochemical activation. As expected, the onset temperature for thermoelectrochemical activation (that is, conversion reaction) is lowered down to 55°C with this ballmilled powder. The conversion reaction evolves as evidenced by the voltage plateau (↓) and the electrode is lithiated by the addition and continuing conversion reaction at 25°C (solid line) after being activated at 55°C.

The formation of nanosized metallic Mo upon lithiation and restoration back to nanosized MoO_2 after delithiation during the 55°C activation period was ascertained from the HR-TEM images and SAED patterns shown in Fig. 6b-e. The points where the images are taken are indicated as * and ** in Fig. 6a. The TEM images taken after lithiation (Fig. 6b) and delithiation (Fig. 6d) illustrate the presence of nanosized particles (<10 nm), which were identified as the metallic Mo and MoO_2 from the lattice fringes (Fig. 6c and e), respectively.

Recently, we have reported the thermoelectrochemical activation behavior of a Cu–In intermetallic compound (Cu_7In_3) that does not show any lithiation activity at room temperature.[24] The activation converts the initial Cu_7In_3 to CuIn phase. A common feature in two systems is that the thermoelectrochemical activation proceeds by two steps. In the first step, the initial phases are transformed to nanosized mixture (metallic Cu/Li_xIn for Cu_7In_3 and Mo/Li_2O for MoO_2) by a conversion-type lithiation. In the second step, more reactive phases (CuIn phase and nanosized MoO_2) are generated in the forthcoming delithiation period. Both of the thermoelectrochemically activated materials are fully lithiated by conversion reaction at room temperature. The literature complains that a lot of metal oxides, phosphides, fluorides, nitrides, sulfides, and intermetallics give a negligible or limited lithiation activity at room temperature even if the reaction is thermodynamically allowed.[11,25-29] Along this line, thermoelectrochemical activation can be utilized as a powerful tool to explore more active materials from those discarded or underestimated materials (for instance, CuIn phase from Cu_7In_3 and nanosized MoO_2 from bulkier one).

Conclusion

This work demonstrates that the kinetically hindered conversion reaction in the MoO_2 electrode can be facilitated either by raising the working temperature or by decreasing the particle size. The onset temperature for conversion reaction shows a rough inverse relationship with the particle size; 85, 55, and <25°C for the raw MoO_2 (0.2–0.3 μm), ballmilled (0.1–0.2 μm), and nanosized (<10 nm) ones, respectively. This can be rationalized by an enhancement in the heterogeneous charge-transfer rate and solid-state

Li^+ or O^{2-} diffusion. A weaker Mo–O bond strength in the nanosized MoO_2 as compared to that for the initial one can also explain the higher conversion reaction activity for this material. The point that should be more highlighted is, however, that the initial MoO_2, which is inactive for conversion reaction at room temperature, becomes active with an excellent cycle performance by thermoelectrochemical activation. The underlying activation mechanism is the generation of nanosized MoO_2 by a simple discharge–charge cycling made at elevated temperatures.

Acknowledgment

This work was supported by the WCU program through KOSEF funded by the Ministry of Education, Science and Technology (no. 400-2008-0230). The authors also acknowledge the Research Center for Energy Conversion and Storage for financial support.

Seoul National University assisted in meeting the publication costs of this article.

References

1. M. Winter, J. O. Besenhard, M. E. Spahr, and P. Novák, *Adv. Mater. (Weinheim, Ger.)*, **10**, 725 (1998).
2. J. M. Tarascon and M. Armand, *Nature (London)*, **414**, 359 (2001).
3. P. Poizot, S. Laruelle, S. Grugeon, L. Dupont, and J-M. Tarascon, *Nature (London)*, **407**, 496 (2000).
4. A. Débart, L. Dupont, P. Poizot, J. B. Leriche, and J. M. Tarascon, *J. Electrochem. Soc.*, **148**, A1266 (2001).
5. D. Larcher, G. Sudant, J. B. Leriche, Y. Chabre, and J. M. Tarascon, *J. Electrochem. Soc.*, **149**, A234 (2002).
6. P. Poizot, S. Laruelle, S. Grugeon, and J. M. Tarascon, *J. Electrochem. Soc.*, **149**, A1212 (2002).
7. T. Ohzuku, T. Kodama, and T. Hirai, *J. Power Sources*, **14**, 153 (1985).
8. J. J. Auborn and Y. L. Barberio, *J. Electrochem. Soc.*, **134**, 638 (1987).
9. J. R. Dahn and W. R. McKinnon, *Solid State Ionics*, **23**, 1 (1987).
10. B. Y. Liaw, I. D. Raistrick, and R. A. Huggins, *Solid State Ionics*, **45**, 323 (1991).
11. H. Li, P. Balaya, and J. Maier, *J. Electrochem. Soc.*, **151**, A1878 (2004).
12. Y. Liang, S. Yang, Z. Yi, X. Lei, J. Sun, and Y. Zhou, *Mater. Sci. Eng., B*, **121**, 152 (2005).
13. Y. Liang, S. Yang, Z. Yi, J. Sun, and Y. Zhou, *Mater. Chem. Phys.*, **93**, 395 (2005).
14. Y. Wang, K. Takahashi, K. Lee, and G. Cao, *Adv. Funct. Mater.*, **16**, 1133 (2006).
15. M. Wagemaker, W. J. H. Borghols, and F. M. Mulder, *J. Am. Chem. Soc.*, **129**, 4323 (2007).
16. L. C. Yang, Q. S. Gao, Y. H. Zhang, Y. Tang, and Y. P. Wu, *Electrochem. Commun.*, **10**, 118 (2008).
17. P. Balaya, H. L. Kienle, and J. Maier, *Adv. Funct. Mater.*, **13**, 621 (2003).
18. S. Grugeon, S. Laruelle, R. Herrera-Urbina, L. Dupont, P. Poizot, and J. M. Tarascon, *J. Electrochem. Soc.*, **148**, A285 (2001).
19. P. L. Taberna, S. Mitra, P. Poizot, P. Simon, and J. M. Tarascon, *Nature Mater.*, **5**, 567 (2006).
20. D. A. Totir, B. D. Cahan, and D. A. Scherson, *Electrochim. Acta*, **45**, 161 (1999).
21. D. Larcher, D. Bonnin, R. Cortes, I. Rivals, L. Personnaz, and J. M. Tarascon, *J. Electrochem. Soc.*, **150**, A1643 (2003).
22. R. Srivastava and L. L. Chase, *Solid State Commun.*, **11**, 349 (1972).
23. K. T. Lee, Y. S. Jung, J. Y. Kwon, J. H. Kim, and S. M. Oh, *Chem. Mater.*, **20**, 447 (2008).
24. Y. S. Jung, K. T. Lee, J. H. Kim, J. Y. Kwon, and S. M. Oh, *Adv. Funct. Mater.*, **18**, 3010 (2008).
25. D. Larcher, L. Y. Beaulieu, O. Mao, A. E. George, and J. R. Dahn, *J. Electrochem. Soc.*, **147**, 1703 (2000).
26. Y. Xia, T. Sakai, T. Fujieda, M. Wada, and H. Yoshinaga, *J. Electrochem. Soc.*, **148**, A471 (2001).
27. J. H. Kim, H. Kim, and H. J. Sohn, *Electrochem. Commun.*, **7**, 557 (2005).
28. M. S. Park, Y. J. Lee, S. Rajendran, M. S. Song, H. S. Kim, and J. Y. Lee, *Electrochim. Acta*, **50**, 5561 (2005).
29. M. D. Fleischauer, M. N. Obrovac, J. D. McGraw, R. A. Dunlap, J. M. Topple, and J. R. Dahn, *J. Electrochem. Soc.*, **153**, A484 (2006).